Interaction of a rigid beam resting on a strong granular layer overlying weak granular soil: Multi-Methodological Investigations

Zuhair Kadhim Jahanger[a,b], S. Joseph Antony[a,1,*], Elaine Martin[a], Lutz Richter[c]

[a] *School of Chemical and Process Engineering, University of Leeds, LS2 9JT, Leeds, UK*

[b] *Department of Water Resources Eng., College of Engineering, University of Baghdad, Al-Jadriya Campus, 10071, Baghdad, Iraq*

[c] *OHB System AG, Munich, Germany*

Abstract: In the geotechnical and terramechanical engineering applications, precise understandings are yet to be established on the off-road structures interacting with complex soil profiles. Several theoretical and experimental approaches have been used to measure the ultimate bearing capacity of the layered soil, but with a significant level of differences depending on the failure mechanisms assumed. Furthermore, local displacement fields in layered soils are not yet studied well. Here, the bearing capacity of a dense sand layer overlying loose sand beneath a rigid beam is studied under the plain-strain condition. The study employs using digital particle image velocimetry (DPIV) and finite element method (FEM) simulations. In the FEM, an experimentally characterised constitutive relation of the sand grains are fed as an input. The results of the displacement fields of the layered soil based DPIV and FEM simulations agreed well. From the DPIV experiments, a correlation between the slip surface angle and the thickness of the dense sand layer has been determined. Using this, a new and simple approach is proposed to predict theoretically the ultimate bearing capacity of the layered sand. The approach presented here could be extended more easily for analysing other complex soil profiles in the ground-structure interactions in future.

*Corresponding author: S. Joseph Antony, E-mail: S.J.Antony@leeds.ac.uk

Key words: Granular mechanics, bearing capacity, layered soil, FEM, DPIV, failure mechanism

Nomenclature

B	Width of the beam (footing)	q_c	Cone resistance
B'	Projection of slip lines on the surface of the bottom layer (Fig. 4)	s_c	Shape factor in the bearing capacity equation for shapes of footing other than a strip footing
c	Cohesion of the soil	S_u	Ultimate vertical settlement of the beam
D_f	Depth of footing embedment	s_u	Shear strength of the clay
D_r	Relative density of the soil	S_R	Resultant displacement
D_{50}	Mean grain size of the soil	S_v	Vertical displacement component
d	Depth of the region M under the beam (Fig. 4)	UBCR	Ultimate Bearing Capacity Ratio
E	Modulus of elasticity	z	Depth of the soil from the beam soil interface
H	Thickness of the top layer of sand	α	Angle of plastic wedge vertices (slip planes) intersecting the horizontal
Kp	Coefficient of passive earth pressure of the top layer of sand	β	Angle of the slip surface
K_s	Coefficient of punching shear	γ	Unit weight of the soil
N_c	Bearing capacity factor due to soil cohesion	γ'	Effective unit weight of the soil
N_q	Bearing capacity factor due to surcharge stress	δ_{bw}	Roughness of the side wall beam interface
N_γ	Bearing capacity factor due to unit weight of soil	δ_p	Roughness of the Perspex wall

P_p	Total passive earth pressure	δ	Roughness angle of the material
$P_{\text{ult layered}}$	Ultimate force for footing on layered soil	θ	Angle of total passive earth pressure
q_{ult}	Ultimate bearing capacity	ν	Poisson's ratio
$q_{\text{ult 1}}$	Ultimate bearing capacity of the top soil	ϕ_1	Angle of internal friction of the top layer
$q_{\text{ult 2}}$	Ultimate bearing capacity of the bottom soil	ϕ_{mob}	Mobilized shear strength
$q_{\text{ult layered}}$	Ultimate bearing capacity for footing on layered soil		

1. Introduction

In the terramechanical engineering applications, we often come across the foundation structures and rigid structural elements interacting with non-homogeneous soil profiles of complex nature. Layered soil profiles are often found either naturally or man-made. Due to the demands of the scarcity of the construction spaces, there is an increasing demand to construct structures on loose soils, which were previously considered as unsuitable for construction (Jahanger et al. 2010). Loose sand packings have high compressibility and low shear strength (Terzaghi et al. 1996). One of the methods to improve the strength of the weak soil is to construct a suitable layer of granular material to decrease the overall compressibility. For instance, oil storage tanks and diesel power stations may be found on a thin layer of compacted granular fill (Jahanger et al. 2010). Unpaved roads are also built on the weak soil where the treated layer of sub bases are used to spread the service loads applied by the passing vehicles (Jahanger et al. 2010). Shallow footings, when built on loose sandy soils, have a low load bearing capacity and undergo large settlements (Terzaghi et al. 1996). Construction on loose sands often requires the utilisation of ground improvement techniques (Das, 2009). Compacted soil layer is used under such foundation structures to improve the ultimate bearing capacity and limit the displacement in the soil. The ultimate bearing capacity equation for sand according to Terzaghi (1943) (as $q_{\text{ult}} = 0.5\gamma B N_\gamma$ where γ, B and N_γ are unit weight of the soil, the width of the footing and bearing capacity factor of the soil respectively) is not directly applicable for layered granular sand.

In a recent study, digital particle image velocimetry (DPIV) was used to understand the displacement fields of strip footing interacting with homogeneous sand bed of different packing densities (Jahanger et al. 2018). The experimental results compared favorably with finite element method (FEM) simulations, which used experimentally measured constitutive relations of the sand grains (Jahanger et al. 2018). The current study deals with the specific case of the bearing capacity of a rigid plane-strain surface beam placed on a layered sand consisting of a dense sand layer overlying a homogeneous bed of loose sand. The study is restricted to cases where the thickness of the top sand layer, *H*, is quantified in terms of the width of the beam, B. A discussion is given of the various theoretical and the experimental work that have been proposed for this type of analysis.

2. Review of the previous work

Numerous researchers have investigated on the ultimate bearing capacity and settlement of the footings interacting with layered soil using theoretical and experimental approaches. Button (1953) was the first to analyse footings on the layered clayey soil. Likewise, many other investigations were conducted for the ultimate bearing capacity of a sand layer overlying a clay layer (Al-Shenawy and Al-Karni, 2005; Burd and Frydman, 1997; Fattah et al. 2011; Khing et al. 1994; Lee et al. 2103; Meyerhof, 1974; Mickalowski and Shi, 1995; Oda and Win, 1990; Okamura et al. 1998; Ramadan and Hussien, 2015). Similar were also conducted for the cases of layered cohesion-friction soils (Azam et al. 1991; Purushothamaraj et al. 1974). Furthermore, researchers have studied theoretically and numerically on the bearing capacity of footings interacting with two-layered granular soils (Farah, 2004; Ghazavi and Eghbali, 2008). Some experimental studies, for example Hanna (1982) focused on the loose sand overlying on dense sand. Most of the aforementioned studies have used simplified failure mechanisms together with a reduction in the mobilized shear strength (ϕ_{mob}) of sand in their corresponding limit analysis and finite element method based simulations. These simplified theoretical mechanisms comprise (i) projected area method (mode 1) that uses constant slip surface angle, β (Fig. 1) (ii) A punching shear failure (mode 2) which assumes zero slip surface angle (Fig. 2) (iii) the theory of bearing capacity by considering the top layer as surcharge (mode 3) and (iv) a variable slip surface method (modes 4 and 5) that assumes different values of β (Figs. 3-4). Large discrepancies between the measured and the predicted values of the ultimate bearing capacity were observed in the above studies. It is worth noting that existing studies either used a constant value of β (Yamaguchi, 1963) or set β =0 (Meyerhof, 1974), but in both cases β is independent of the thickness of the top layer (*H*). However, other conclusions from the previously mentioned studies are that the ultimate bearing capacity for the layered soils depends on the individual shear strength parameters of each layer, thickness of the top layer (*H*), the width of the footing (*B*), the shape and the depth of footing embedment (D_f in Fig. 2) and (*H/B*) thickness ratio of the top layer to the width of the footing (Fig. 1).

2.1 Theoretical work

The most widely used methods to calculate the bearing capacity of layered soil are the projected area method (Yamaguchi, 1963) and the punching shear failure method (Meyerhof, 1974). The former method has been adopted by many researchers and used a constant value of β (Fig. 1) in their studies; for example, 30° by Yamaguchi (1963), 30° and 45° by Myslivec and Kysela (1978) and considered equal to the angle of internal friction (ϕ_1) of the top layer of the soil by Baglioni et al. (1982). The latter, the punching shear failure, assumes as β=0 for the actual failure surface, but accounted for the shear strength of soil along the vertical wedge of the slip plane.

In the following, the principles behind the different methods are discussed briefly. In the projected area method, a rigid block of truncated cone under the footing was assumed in the top layer as well as a constant slip surface angle β (Fig. 1). The shear strength along the slip surface of the top layer was neglected. The ultimate bearing capacity for the strip footing resting on the sand layer overlying clay could be estimated from the shear strength of the underlying clay soil and the dimension of the base of the trapezoidal failure pattern according to Yamaguchi (1963) (as, $q_{\text{ult layered}} = ((1 + 2H\ tan\beta)/B)q_{\text{ult 2}}$ where, $q_{\text{ult layered}}$ is the ultimate bearing capacity for footing on layered soil as a whole and $q_{\text{ult 2}}$ is the ultimate bearing capacity of the underlying clay soil (Fig.1)). Therefore, the ultimate bearing capacity for a surface strip footing (D_f=0) resting on the layered granular soil of cohesion c=0, and subjected to the vertical load can be expressed by neglecting the N_q (bearing capacity factor) contribution (Dijkstra et al. 2013; Jahanger et al. 2018). Based on the mode 1, the bearing capacity for the dense sand on loose sand can be written as:

$$q_{\text{ult layered}} = 0.5\gamma_2 B N_{\gamma 2} + H\ tan\beta\ \gamma_2 N_{\gamma 2} \tag{1}$$

in which β is assumed as 30° (Yamaguchi, 1963), γ_2 and $N_{\gamma 2}$ are unit weight and bearing capacity factor of the bottom soil layer respectively.

The traditional analytical analysis according to Meyerhof (1974) studied the case of a dense sand resting on a soft clay. The failure of a rigid continuous footing punching through a thin layer of dense sand into a thick underlying deposit of clay was assumed as an inverted uplift problem. The failure mode 2 (Fig. 2) considered a sand mass having an approximately truncated pyramidal shape, pushing into the lower layer in the direction of applied load. Similarly, Hanna (1981) studied mode 2 punching failure surface (β=0) of strip footing on a strong sand overlying weak sand deposit (Fig.2). Meyerhof (1974) proposed a theoretical equation for bearing capacity by considering the failure method using the assumed plane of failure, i.e. vertical side block (β =0) instead of the trapezoidal shape (P_p in Fig. 2 is the total passive earth pressure) for layered dense sand overlying loose sand. The bearing capacity of the layered soil was evaluated from the force limit equilibrium of the sand block, and approximated as follows for mode2:

$$q_{\text{ult layered}} = 0.5\ \gamma_2\ B\ N_{\gamma 2} + (\gamma_1 H^2\ \mathrm{K_s}\ tan\,\phi_1)/B - \gamma_1 H\ \leq q_{\text{ult 1}} \tag{2}$$

where, $q_{\text{ult 1}}$, γ_1 and ϕ_1 are ultimate bearing capacity, unit weight and peak friction angle of the top soil layer respectively. In this, $\mathrm{K_s} \tan \phi_1 = \mathrm{Kp} \tan \theta$ and ϕ_1 is experimentally measured value of the angle of internal friction of the top layer. $\mathrm{K_s}$ =6.5 pertaining to the value of ϕ_1 and $q_{\text{ult 2}}/q_{\text{ult 1}}$. θ is the mobilized angle of shear resistance on the assumed failure zones (Fig. 2). Kp is coefficient of passive earth pressure of the top soil.

Okamura et al. (1998) have proposed a new limit equilibrium method in order to verify the validity of the previous modes by comparing them with the centrifuge test results. They have adopted a failure mechanism as shown in Fig. 3 which is similar to the existing methods with accounting for the shear strength along the shear slips surfaces. In their analysis, β is calculated using the limit equilibrium method (Okamura et al. 1998).

2.2 Experimental work

Hanna (982) suggested to calculate the ultimate bearing capacity of the layered soil of weak sand overlying a strong deposit by considering the top layer as surcharge (mode 3) using the following:

$$q_{\text{ult layered}} = 0.5\,\gamma_2 B N_{\gamma 2} + \gamma_1 H N_{q2} \leq q_{\text{ult 1}} \qquad (3)$$

In this, the ultimate bearing capacity of the layered soil (Eq. 3) is the sum of the bearing capacity of the lower layer 2, and the shearing resistance in the top sand layer 1 of thickness *H*. This can be considered as the ultimate bearing capacity for the strip footing according to the Terzaghi's bearing capacity equation (Terzaghi, 1943).

Farah (2004) has theoretically calculated β based on the experimental results of Meyerhof and Hanna (1978). In this, the angle β was correlated with the thickness ratio *H/B* for varying between 0.5 and 5, and the ratio $q_{\text{ult 2}}/q_{\text{ult 1}}$ =0.08. The variation of the angle β according to the analytical results of Farah (2004) is constant (89°) up to *H/B*=1.0, then β gradually decreases with depth to β =40.1° at *H/B* = 4.5, before β increases to 46.6° when *H/B*=5.0.

It seems that β was overestimated as Prandtl (1920) and Terzaghi (1943) have showed that the maximum value of β is equal to $45 + \phi/2$ which results, β =68.85° even when *H/B* tends to zero.

In a preliminary study conducted by Jahanger et al. (2016), DPIV was used to investigate the failure plane of a soil system of a dense sand layer on loose sand. It was noted that the measured value of β significantly depended on the depth of the dense sand layer. The schematic diagram of their failure plane of the layered soil system is presented in Fig. 4. However no quantification of β, as well as its use in evaluating the ultimate bearing capacity of layered system were reported either. These form the motivation of the current work. For this, a new methodology is presented below based on the experimentally measured β for the layered soil system considered in this paper. Furthermore, finite element analysis of the common cases were performed here for the purpose of comparisons.

3. Materials and experimental methods

3.1 Soil samples

The soil used here are dry silica sand samples obtained in UK. Sand properties were characterised according to the American Society for Testing and Materials (ASTM, 1989; Head, 2006). Their experimentally measured material properties and grain size distribution are provided in Table 1. The roundness of the sand grains were mostly spherical to sub-prismoidal and the angularity of the grains were characterised as angular and sub-angular (Head, 2006). For this, digital microscopy images of the grain samples were used. These data revealed that the soil chosen is classified as poorly graded (SP) according to the Unified Soil Classification System (Cerato and Lutenegger, 2007; Dijkstra et al. 2013; Jahanger et al. 2018; Liu and Iskander, 2004).

Table 1 Experimentally measured physical properties of the sand used.

Type of sand	**Loose**	**Dense**	**Standards**
Dry density (γ_d): (kN/m^3)	14.70	15.80	ASTM C29/C29M
Void ratio (e_o)	0.76	0.64	
Relative density, D_r : % ± 2%	24	72	ASTM C128
Peak angle of internal friction, ϕ_{peak} : °	32	44.3	ASTM D4767
Residual angle of internal friction, ϕ_{cr}: °	30	36.3	Head (2006)
Max. dry density (γ_{dmax}): kN/m^3	16.50		ASTM D698
Min. dry density (γ_{dmin}): kN/m^3	14.23		ASTM D4254 method C
Max. void ratio (e_{max})	0.83		ASTM C29/C29M
Min. void ratio (e_{min})	0.58		ASTM C29/C29M
D_{10} : mm	0.25		
D_{30} : mm	0.31		ASTM D421
D_{50}: mm	0.37		ASTM D422
D_{60} : mm	0.40		
Uniformity coefficient, C_U	1.55		ASTM D2487
Coefficient of curvature, C_C	0.93		
Angle of repose of the sand, °	34		ASTM C1444

Bearing capacity of the rigid beam was tested using an aluminum planar test box of 460 mm in length, 250 mm in height and 39 mm in thickness, filled with dry sand (Fig. 5). The box had transparent and smooth Perspex front wall of 15 mm thickness and also 10 mm Aluminum back wall to eliminate any bending effects during the test in the plane strain direction. The authors also verified that under the ultimate load (P_{ult}) of the dense sand packing (*H/B*=6.5) did not lead to any remarkable out of plane movement of the container's face as this was checked using a dial gauge (0.01mm resolution) mounted to the side walls from a magnetic base (though the picture of this arrangement is not included here). The rigid beam base was relatively rough (ratio between the angle of interfacial friction of the rigid beam and angle of internal friction of the sand (δ/ϕ) is less than 0.25). The relative roughness of the side wall of the beam in contact with Perspex wall (δ_p/δ_{bw}) was 0.09, which is very small and negligible. The beam dimensions were of 38 mm × 38 mm× 15 mm. The ratio of the width of the beam to D_{50}; i.e., $B/D_{50} \geq 100$ (which is within the permissible limit (Dijkstra, et al. 2013; Lau, 1988)) to avoid any scale effect arising from the relative sizes of the beam and sand grains. The model dimensions used here are widespread and have been used in previous research scenarios of beam-soil interactions (Bowles, 1996; Jahanger et al. 2018; Lemmen et al. 2017; Raymond and Komos, 1978). To minimize any frictional effects of the rigid beam with the wall, a small gap of 1 mm was allowed between the rigid beam and the back aluminum wall, so that they do not affect the deformation of the soil recorded by DPIV at the front of the planar box so that the load was transferred from the beam to the soil grains rather than to the wall. These measures ensured that the observed movement from the images is due to the inner movement in the grains under mechanical loading (White and Bolton, 2004).

3.2 Preparation of the samples

For the case of homogeneous packing (non-layered system), two cases of relative densities (D_r) of sand (loose and dense) were considered here. The loose granular packing (H/B=0 in Fig. 5(b), γ_{loose}=1500 kg/m^3, D_r = 24 % ± 2) was prepared by pouring the sand grains uniformly across the width of the box in small layers using pluviation technique (Kumar and Bhoi 2009) so that any segregation of the grains was avoided during the construction process. The top surface of the sand layer was gently levelled off using a hand scraper. Care was taken not to disturb the constructed loose sample in any way before applying the axial loading in our experiments. The mass of the sand grains laid in the test box to the required height pertains to the required density of the loose sample. The dense packing (H/B=6.5 in Fig. 5(b), γ_{dense}=1610 kg/m^3, D_r =74 % ± 2) was achieved by compacting the sand in five equal layers, and using 60 blows in 0.035 m lifts per layer with a 0.0016 m^2 compaction hammer of 1.05 kg weight (Cerato and Lutenegger, 2007; Jahanger et al. 2018; Lavasan and Ghazavi, 2012).

Layered samples of dense sand overlying loose sand were prepared by compacting the dense sand first inside the bottom of the test box. Then the loose sand was poured using pluviation technique (Kumar and Bhoi, 2009) after which the box was turned upside down using a simple mechanical apparatus designed for this purpose. A wide range of *H/B* was considered: $0.5 < H/B < 6.5$. At first the dense sand layer was compacted into the bottom of the test box to the required depth *H/B*, as explained earlier (Cerato and Lutenegger, 2007; Jahanger et al. 2018; Lavasan and Ghazavi, 2012). The bottom plate of the box has a slightly smaller dimensions than the maximum available dimensions of the box, i.e., less by 1.5 mm from all three sides (except the front side through which DPIV measurements were made). This would help to remove the bottom plate from the box after turning the box upside down easily without much disturbances when required at a later stage. However, to avoid any leakage of sand grains when reversing the box, this small gap was initially covered using a cellophane type. After this, the loose sand layer was poured in layers on the dense sand as discussed above. Then, the top plate (plan area is equal to the allowable plan area) was fixed to the box with screws. Then, the test box was turned upside down. Hence the top layer of the sample contains the dense sand and the bottom layer contains the loose sand. The authors also verified that there was no significant diffusion of sand particles from the top layer through the interface to the bottom layer of sand packing, by initially color-coating the interface region of the sand layers (Fig. 5c). Even after reversing the test box as explained earlier, the level of the color-coded interface layer of sand remained practically horizontal (Fig. 5c). The beam was placed symmetrically on the top surface of the layered sand bed through which the axial loading was applied in the experimental study. This study considered different cases of layered soil, viz., H/B = 0, 0.5, 1.0, 2.0, 3.0, 4.0, 6.5. In this, H/B = 0 means a single layer of homogeneous loose sand packing and H/B = 6.5 pertains to practically a single layer of homogeneous dense sand packing. For other cases of layered sand, the total sand depth (6.5B) was held constant, but the thickness of the dense sand layer (H) was varied systematically as H/B = 0.5, 1.0, 2.0, 3.0 and 4.0. Hence, any boundary effects from the bottom rigid wall of the box was practically negligible. Furthermore, the dimensions of the test box was kept much greater than that of the beam (Fig. 5b) to minimize boundary effects.

3.3 Digital particle image velocimetry analysis

Particle image velocimetry (PIV) is often used in the field of fluid mechanics to track the motion of fluid flow using tracer particles (Adrian, 1991). It has been also used to study the displacement and(/or) strain distribution in some cases of granular materials (Hamm et al. 2011; Murthy et al. 2012; Willert and Gharib 1991). Recently, PIV has enabled to obtain a high resolution measurement of soil deformation in geotechnical engineering problems (Cheng et al. 2001; Hamm et al. 2011; Jahanger et al. 2018; O'Loughlin and Lehane 2010). In the present study the field of view of the PIV camera focused on the beam-soil interaction region was 270 mm×180 mm, which was further sub-divided into 375000 interrogation areas of 8×8 pixels each covering a zone of about 0.4 mm × 0.4 mm. Nikon D5500 high definition camera (6000 × 4000 pixels) was used here. This corresponds to a scale of ~ 0.045 mm per pixel in this study. DPIV pertains to the digital platform of particle image velocimetry (Jahanger et al. 2018).

3.4 Experimental tests

An axial compression loading was applied slowly on the beam (0.05 mm/s penetration rate) using Instron loading machine with 5 kN/0.1N resolution (Fig. 5a). The loading machine also had an inbuilt linear variable differential transformer (LVDT) to measure the settlement of the indenting beam on the layered packing. The macroscopic load and settlement of the beam were also recorded from the tests. The Nikon D5500 high definition camera (6000 × 4000 pixels) was fixed in front of the box and two light sources were used to illuminate the rig. However, as the loading condition is quasi-static in this study, an image at every 10 seconds was found to be adequate until reaching the failure load of the sand packing. Dynamic Studio Software Platform (DSSP) was used to analyse the digital images acquired during test using DPIV (Dynamic Studio, 2013). This functionality built in the DPIV was used well to analyse the digital frames of the grains, and to calculate velocity vectors of the grains and their evolution during load application within the sand layer (Albaraki and Antony, 2014; Jahanger et al. 2018). The distribution of velocity vectors of the grains was examined for which an adaptive interrogation area (IA) of maximum size 64 × 64 pixels in 8 × 8 grid step size resolution was employed in the image analysis. A typical mean size of sand grain (D_{50} = 0.37 mm) was represented by about 8×8 pixels (patch). Each of these patches was tracked using an adaptive PIV method, to identify the movement field of soil between consecutive images obtained from the front side of the Perspex sheet of the test rig, to a measurement precision of 0.05 mm for the field of view used during these experiments. The adaptive PIV iteratively adjust the size of the individual interrogation areas (IA) in order to adapt to local seeding densities and flow gradients (Dynamic Studio, 2013; Jahanger et al. 2018). This space-pixel dimension of the measurement was calibrated by printing a known scale on the test box along the horizontal and vertical directions. White et al. (2003) have shown that the precision of the measurement (i.e., the random difference between multiple measurements of the same quantity) improves with larger PIV patches and it is inversely proportional to the amount of the measurement resolution. This size of the mesh patch used here corresponds to a precision better than 1 pixel. It was verified that the variation in image scale in both horizontal and vertical direction were not significantly different. Hence the measurements made here are at the local-scale (close to discrete-grain scale) rather than a continuum measure. The tests were repeated at least two times to verify the repeatability and the consistency of the test data (Kumar and Bhoi 2009).

Though the results are not presented here, two standard cone penetration test tests (CPTs) were also conducted for each soil density to verify the relative density of single layer sand using a 10 mm diameter model CPT (Dijkstra et al. 2013; Jahanger et al. 2018; O'Loughlin and Lehane, 2010). The CPT was inserted at a penetration rate of 1 mm/s in the current experiments. The penetration resistance (Cone resistance = q_c) profiles are plotted against the penetration depth (z) from the bottom level of the beam. As the authors expected, the penetration resistance of dense sand was higher than that of the loose sand. The penetration resistance of loose sand remained almost constant with depth after z/B =2.5, but the penetration resistance for dense sand increase with depth at an increasing rate (kPa/mm). The rate of the penetration resistance in kPa/mm of dense sand was larger than that of the loose sand. Again, the differences in the penetration resistance for different relative densities are primarily accounted for the relatively larger volumetric compressibility in loose sand than the dense sand (Jahanger et al. 2018). The cone resistance of dense sand layer overlying loose sand samples started to decrease when the cone penetrometer approached the underlying loose sand layer. The error in the CPTs measurements of the samples of different cases of sand bed conditions was within 5%.

4. FEM simulations

Non-linear elastic finite element simulations have been performed for the cases of a single rigid beam indenting into layered dense sand on loose sand packing using ANSYS workbench 17.2 version. ANSYS is a broad purpose FEM package for numerically solving a wide variety of mechanical interactions (ANSYS, 2016).

In the present FEM study, the simulations were performed using ANSYS by creating a 2D solid geometry of the beam and the layered soil. The soil and the beam were modelled as under plane strain condition. The discretization of the beam and the layered soil were done using an eight-nodded quadratic solid element having two degrees of freedom at each node, i.e., translations in the nodal x and y directions (Fig. 6). The nodes and element numbers are equal to about 80000 and 25000 respectively. The chosen domain along with applied boundary conditions is shown in Fig. 6.

The simulations were held under identical boundary conditions for beam indenting with different H/B. In the simulations, the bottom most nodes have been constrained in both horizontal (S_h) and vertical directions (S_v) (S_h=S_v = 0). A line of symmetry was used along the beam centre line (S_h=0, $S_v \neq$0). The vertical far side of the assembly was fully constrained in the horizontal direction, S_h=0 and free to move in the vertical direction $S_v \neq 0$ (Jahanger et al. 2018; Mosadegh and Nikraz, 2015). The contact regions between the beam and the sand were modelled as a relatively rough surface (interface friction coefficient=0.25) corresponding to the experimental study (Jahanger et al. 2018; Lee, 2015). This interaction involves displacements and sliding of the elements in the contact region, which introduces non-linearity to the system. The contact regions between the sand layers were modelled as well bonded (Mohsenimanesh et al. 2009). A refined mesh was generated at the beam-soil interface where the largest stresses and strains would be expected. It should be mentioned that Skewness mesh metric (a measure of mesh quality) of 0.001 maximum value was obtained which is acceptable (Lee, 2015). The size of the elemental geometry is shown in Fig. 6.

The material model for the soil describes the nonlinear plasticity behaviour, which corresponds to the actual soil properties used in the current ANSYS simulations. For this, the experimentally characterised bulk stress-strain relationship corresponding to the load-displacement curves of loose and dense sand presented in Fig. 7 were discretised into a large number of linear segments and fed as user defined digital input (ANSYS, 2016; Jahanger et al. 2018; Lee 2015; Mohsenimanesh et al. 2009) to account for the corresponding materials properties of the layered sand. Furthermore, the experimentally characterised material physical properties were used i.e. unit weight of the soil (γ), modulus of elasticity (E) and typical value of Poisson's ratio (ν) for sand (E = 25 MPa and 50 MPa whereas ν=0.2 and 0.35 for the loose and dense sands respectively (Das, 2009)). In the present analysis, ANSYS used the multilinear isotropic hardening of the stress-strain relation (Jahanger et al. 2018; Lee, 2015). Geometrical non-linearity was also allowed in the simulation (ANSYS, 2016). The axial loading was applied on the rigid beam geometry elements. The evolution of displacement components in the soil elements was tracked under different loading levels and compared with corresponding DPIV measures later.

5. Results and discussions

The experimental axial load–settlement results for a typical beam interacting with homogeneous (single layer) and layered sand are presented in Fig. 7. The load-settlement curves characterised here provide a consistent response with respect to an increase in the height of the dense sand layer (*H*). A well-defined peak is obtained for the case of *H/B*= 6.5 (practically a homogeneous dense sand packing). Using the load-settlement data, the tangent intersection method (Akbas and Kulhawy, 2009) was applied to measure the value of the ultimate bearing capacity (Fig. 7). This involves linear curve fittings for the initial loading and hardening phases of the load–settlement relations. The intersection point of these two lines thus corresponds to the q_{ult} (Fig. 7). The ratio of the ultimate bearing capacity of the loose sand (*H/B*= 0) to the ultimate bearing capacity of the dense sand (*H/B*= 6.5), $q_{\mathrm{ult}\,2}/q_{\mathrm{ult}\,1}$ =0.08. However, in the case where there was not a clear curvature in the shape of the load- settlement plots, the failure corresponds to punching failure (e.g. test *H/B*= 0 – 2.0) (Vesic, 1973). However, the failure surface was totally located in the dense soil layer if the depth *H* is relatively large (*H/B* > 2.0) and eventually resulted a soil rupture (Shaaban, 1983).

The ratios of ultimate vertical settlement of the beam (S_u) to the width of the beam (*B*), S_u/B for the case of homogeneous sand are 6% and 8% for the dense and loose sand respectively. In the cases of layered sand, this varies between 14%-18% respectively. These measures and the nature of bulk load-settlement curves are consistent with Das (2009) for homogeneous sand, and Meyerhof and Hanna (1978) for layered sand. The authors wish to point out that, in the case of strip footings used in practice, 3D condition could exist around the ends of the strip footings even if the footing is long. However, for most parts of long strip footings, plane-strain condition could exist (Bowles, 1996; O'Loughlin and Lehane, 2010; White and Bolton, 2004) as assumed in the current 2D plane-strain experiments (Jahanger et al. 2018; Raymond and Komos, 1978).

Figure 8 presents the effect of depth of the dense sand layer overlying loose sand bed on the evolution of the mean resultant velocity vectors ($\boldsymbol{S_R} = \sqrt{\boldsymbol{S_v^2} + \boldsymbol{S_h^2}}$) beneath a rigid beam subjected to the ultimate load were measured from PIV data. It is evident that, for the homogeneous loose sand (*H/B*= 0), the slip planes occurs in a triangular wedge shape through the punching shear failure mode (Vesic, 1973).

For the case of homogeneous dense sand (*H/B* ≥ 4.5) the initial triangular wedge (punching failure) is followed by the formation of active and passive failure zones (marked as zones 1-3 in Fig. 8). The authors had also observed that outside zone-1, the particles tended to move downward and sideward symmetrically until the ultimate bearing capacity was reached. Similar trends were noticed in other cases reported by Jahanger et al. (2018), Murthy et al. (2012), Prandtl, (1920) and Terzaghi (1943). The depth of this plastic wedge at the ultimate bearing load is equal to about B, whose vertices (slip planes) intersect the horizontal at an angle (α) of about ($\phi < \alpha = 56° < 45 + \phi/2$). These are consistent with Terzaghi's assumption (1943) for relatively rough footing, which have not been confirmed using microscopic experiments, but using DPIV here. Furthermore, Kumar and Kouzer (2007) have assumed similar measures for using plasticity limit analysis of homogeneous soil using FEM. The current experimental study supports such an assumption.

Surprisingly, in the case of layered packing, the slip planes are dominantly through the punching mode, but the shape of the slip planes contains a distinct rectangular wedge supported by a semi-circular (or simplified triangular) wedge (Fig.8). Furthermore, the sand surface does not heap noticeably on both sides of the beam (Fig. 8) for the case of layered sand. This profiles corresponds to the theory of punching shear failure that occurs in the top dense sand layer, followed by another punching shear failure in the bottom soil layer in the cases of *H/B* ≤ 1. However, the authors have observed that if *H/B* ≥ $4B$, then the failure mode was fully located within the top soil layer, which is the upper bound for the ultimate bearing capacity of dense sand (Fig. 7, *H/B* ≥ 4.0).

For the analysis of failure of wedge materials indented by a rigid beam, Prandtl (1920) assumed that the failure occurs along definite slip surfaces (lines) in the material beneath the indenter. Under plastic equilibrium, a rigid triangular wedge of soil was formed below the indenter with base angle $\alpha = 45 + \phi/2$ (Fig. 8). Further, the soil mass on the left and right of the rigid triangular wedge extended radially outwards (zone 2) and upward (zone 3) along the boundaries of the plastic flow as shown in Fig. 8. So, Prandtl- type slip lines commonly appear in the tests on homogeneous sand if the beam is loaded greater than the ultimate load (Oda and Win, 1990). In the series of layered sand, however, two slip lines starting from the beam edges expand downward with angle β (Fig.8). It seems that the angle β depends on the angle of internal friction of the dense sand as well as its thickness *H* (*H/B* ≥ 1.0), inconsistent with the theoretical work of Burd and Frydman (1997) for a uniform sand overlying a thick bed of clay (*H/B≤1.0*). Burd and Frydman (1997) stated that the value of β is insensitive to the top thickness of the sand layer.

The associated plastic strain in the rectangular mass sand is concentrated in a shallow zone right under the beam. The depth of such sand mass (M) is equal to about 0.3-0.5*H*. As the beam compresses, the displacement of the grains occurs generally downwards, with the soil element trajectory moving towards the deeper loose soil interface. In contrast to ultimate bearing capacity theory which comprises soil heave around beam edges to accommodate the punch volume, the mean resultant velocity vectors beneath the beam at ultimate load is dominantly downwards. Larger net downward displacement and less lateral displacement are observed in layered soil than in the case of homogeneous sand.

6. Comparison of the DPIV measurements with FEM analysis

Here the typical results are presented below for the case of rigid beam interacting with the layered soil of dense sand on loose sand packing for the case of *H/B*= 0.5 (Fig. 9). This shows the comparison of mean resultant displacement profile and vertical displacement component contours using DPIV and FEM (ANSYS) analysis for the case of beam interacting with layered soil system under the ultimate load. It is evident that a good level of agreement is obtained between the DPIV and FEM results both qualitatively and quantitatively. Furthermore, though the figures are not presented here, the authors had performed the FEM analysis for the other cases of soil profiles reported in this study, and a good level of agreement of the displacement measures were obtained with that of DPIV experiments. The results obtained from the current DPIV experiments with those obtained from ANSYS simulations are presented in Table 2 for comparison purposes. As seen, the results obtained here from the current FEM analysis are in an excellent agreement with those obtained from ANSYS analysis for different cases of layered sand.

Table 2 Comparison of ultimate load results obtained from current DPIV experiments with FEM.

Width of the beam (mm)	H (mm)	H/B	Ultimate load P_{ult} (N)		
			Current DIPV experiments	FEM	Error %*
38	0	0	40	42	+5
	19	0.5	50	48	-4
	38	1.0	67	71	+5.9
	76	2.0	90	95	+5.5
	114	3.0	115	117	+1.7
	152	4.0	145	148	+2.1
	247	6.5	170	175	+3.0

$* \, Error\ (\%) = ((FEM - Exp.)/Exp.) \times 100$; (+) overestimated, (-) underestimated

7. New proposed method

By taking advantage of the experimentally characterised failure surfaces using DPIV (Fig. 4), here the authors propose a new method for evaluating bearing capacity of the layered soil system encountered here. The displacement of the loose sand located at shallow depth below the rigid beam is independent of the distribution of the pressure on the base of the beam itself, because the dense layer supporting the rigid beam acts as a natural raft that distributes the load from the beam to the loose sand layer (Terzaghi et al. 1996). Nevertheless, the displacement might be considerable at the interface of dense and loose layered sand media. This failure mechanism is kinematically realistic (Fig. 8). The whole soil media (Fig. 4) can be bounded by failure envelopes 1-3 (Fig. 4, *abcd* region) through beam's corners and a semi-circle profile in the loose sand media. Inside zone *abcd*, the displacement occurs mostly vertically. Hence, this is the lower boundary of the zone of plastic equilibrium (Terzaghi, 1943).

As observed from Fig. 8, β varies with the depth of the dense sand layer. Therefore, a relation between β and *H/B* from the DPIV measures (Fig. 10) has been presented in Eq. (4). The lower bound solution is obtained when β = 0 which corresponds to no lateral dilatancy of the failure region (same as mode 2, Meyerhof, 1974). An upper bound solution is obtained when $\beta = \phi_1$ which corresponds to an associated flow rule where the angle of dilation (ψ) equals the angle of internal friction of dense sand. However, the plots of the mean resultant velocity vectors beneath the beam at ultimate load for different *H/B*, show that the angle β is variable and depending on *H/B* and the angle of internal friction of the top sand layer ϕ_1 (Fig. 10). The trend of the fitted curve is consistent qualitatively with theoretical work of Farah (2004) for *H/B*. So, from the test data used in Fig. 10, a third order polynomial equation was obtained as it was the best fit using the regression analysis as follows:

$$\beta / \phi_1 = -0.011\,(H/B)^3 + 0.115\,(H/B)^2 - 0.255\,(H/B) + 1.041 \quad (4)$$

According to Figs. 4 and 10 and the analysis according to Terzaghi et al. (1996) for shallow foundation ($D_f/B \leq 4.0$ (Das, 2009)), the authors present a new set of equations for mode 4 for as:

$$q_{\text{ult layered}} = 0.5\, B\, \gamma_2 N_{\gamma 2} + \gamma_1 H N_{q2} \leq q_{ult\,1} \quad (5)$$

By using $B = B'$ here (Fig. 4)

$$q_{\text{ult layered}} = 0.5\,[B + 2H\tan\beta]\;\gamma_2 N_{\gamma 2} + \gamma_1 H N_{q2} \leq q_{ult\,1} \tag{6}$$

$$q_{\text{ult layered}} = 0.5\,B\,\gamma_2 N_{\gamma 2} + H\tan\beta\;\gamma_2 N_{\gamma 2} + \gamma_1 H N_{q2} \leq q_{ult\,1} \tag{7}$$

For comparison purposes, the authors also performed the analysis for mode 5, using Eq. 1 (mode 1) but with variable slip surface angle β measured from the current DPIV test results. Here the authors present a detailed comparison of the bearing capacity of layered soil system based on modes 1-5 with the current DPIV-based experimental results in Fig 11 (a) and (b). N_γ and N_q for loose and dense sand are obtained corresponding to their ϕ_{peak} using (Terzaghi, 1943). To compare the performance between each approach, a non-dimensional parameter which is the ultimate bearing capacity ratio (UBCR) was used to analyse the results (Binquet and Lee, 1975). UBCR is defined as the ultimate loads ($q_{\text{ult layered}}$) of the rigid beam on layered soil system divided by the ultimate load of the same rigid beam on homogeneous dense sand ($q_{\text{ult 1}}$). It can be observed that the projected area method (mode 1) highly underestimates the bearing capacity of the layered media due to ignoring the shearing resistance of the soil along the sand slip surfaces and the use of a fixed slip surface angle β = 30° in mode 1. The results based on mode 2 (Meyerhof, 1974) gives a conservative value for the bearing capacity due to use of an assumed plane of failure (with β = 0, Fig. 2). The results based on mode 3 (Hanna, 1982) reveals a conservative estimate of the UBCR. However, the results based on the newly proposed method (mode 4) compare well with the current experimental values of UBCR.

It is interesting to note that mode 5 gives a relatively more comparable trend with the experimental results of UBCR than using modes 1-3. It is also interesting to note that, the UBCR reaches a value of 1.0 (Fig. 11 (b)) for different values of *H/B* of the layered sand (as well as depending on the mode of analysis used). For example, to achieve UBCR=1.0, modes 1-5 predicted the required value of *H/B* as ~11.5, 5.5, 6.0, 3.5 and 4.7 respectively. The results of mode 4 and mode 5 are closest to what is commonly considered in geotechnical engineering application (*H/B*= 4-5).

8. Conclusions

In this study DPIV is used to understand the local and global geomechanical characteristics of rigid beam interacting with layered sand deposit in a coherent manner. Where possible, the displacement measures and generic characteristics of velocity fields in the layered sand are compared with FEM and a good level of agreement is obtained. Failure surfaces of homogeneous sand are consistent with Vesic (1973) but the advanced measurements reported here detect their evolutions more precisely. The boundaries of the zone of plastic flow in dense sand overlying loose sand at failure load measured here are remarkably similar to the shape of such intuitive diagrams suggested by Meyerhof (1974), but with different values of β.

The new modified Eq. (7) makes it possible to estimate the bearing capacity of the layered granular soil with quite a good level of accuracy. However, the results obtained from these model tests and new proposed approach (mode 4) can be applied for most strip prototype especially when $B \leq 1.0$ m (Jahanger and Antony, 2017). Therefore, based on the results reported here, DPIV could be applied in future to develop robust failure surfaces for more complex soil profiles and foundation types researches encounter in geotechnical engineering applications. The obtained layered failure mechanisms could be employed in a related theoretical solutions in the future.

Acknowledgments

ZKJ acknowledges the Ministry of Higher Education and Scientific Research (MOHESR), Republic of Iraq and the University of Baghdad for the doctorate scholarship (Grant No. 2075 in 15-05-2013).

References

Adrian, R. J., 1991. Particle-imaging techniques for experimental fluid mechanics. Ann. Rev. Fluid Mech. 23, 261-304.

Akbas, S. O., Kulhawy, F. H., 2009. Axial compression of footings in cohesionless soils. I: Load-settlement behavior. J. Geotech. Geoen. Eng. 135, 1562-1574.

Albaraki, S., Antony, S. J., 2014. How does internal angle of hoppers affect granular flow? Experimental studies using Digital Particle Image Velocimetry. Powd. Tech. 268, 253-260.

Al-Shenawy, A. O., Al-Karni, A. A., 2005. Derivation of bearing capacity equation for a two layered system of weak clay layer overlaid by dense sand layer. Pertanika J. Sci. Tech. 13, 213-235.

ANSYS 17.2, 2016. ANSYS Theory Manual. ANSYS, Inc., Canonsburg, Pennsylvania, USA.

ASTM, 1989. American Society for Testing and Materials, Soil and Rock, Building, Stores, Geotextiles, ASTM Standard, 04.08.

Azam, G., Hsieh, C. W., Wang, M. C., 1991. Performance of strip footing on stratified soil deposit with void. J. Geo. Eng. 117.5, 753-772.

Baglioni, V. P., Chow, G. S., Endley, S. N., 1982. Jack-up rig foundation stability in stratified soil profiles, Proc. fourteenth Offshore Tech. Conf. 4.

Binquet, J., Lee, K. L., 1973. Bearing capacity tests on reinforced earth slabs. J. Geotech. Eng. Div. 101, 1241-1255.

Bowles, J.E., 1996. Foundation Analysis and Design, fifth ed. McGraw-Hill, Singapore.

Burd, H., Frydman, S., 1997. Bearing capacity of plane-strain footings on layered soils. Can. Geo. J. 34 (1997), 241-253.

Button S. J., 1953. The bearing capacity of footings on a two-layer cohesive subsoil. Proc. third Int. Conf. Soil Mech. Found. Eng. Zurich, 1, 332-335.

Cerato B., and Lutenegger A. J. 2007. Scale effects of shallow foundation bearing capacity on granular material. J. Geotech. Geoenviron. Eng. 133, 1192-1202.

Cheng, Y., White, D. J., Bowman, E. T., Bolton, M.D., Soga, K., 2001. The observation of soil microstructure under load. Powd. Grain, Balkema, 69-72

Das, B. M., 2009. Shallow Foundations: Bearing Capacity and Settlement, second ed. CRC Press, London.

Dijkstra, J., White, D. J., Gaudin, C., 2013. Comparison of failure modes below footings on carbonate and silica sands. Int. J. Phys. Model. Geotech. 13, 1-12.

Dynamic Studio, 2013. Dynamic Studio User's Guide. Dantec Dynamics, Skovlunde, Denmark.

Fattah, M. Y., Rahil, F. H., Turki, M. A., 2011. Determination of the adequate thickness of granular subbase beneath foundations. Eng. Tech. J. 29, 1845-1869.

Farah, C. A., 2004. Ultimate Bearing Capacity of Shallow Foundations of Layered Soils, M. Sc. Thesis, Concordia University, Quebec: Concordia, Canada.

Ghazavi, M., Eghbali, A. H., 2008. A simple limit equilibrium approach for calculation of ultimate bearing capacity of shallow foundations on two-layered granular soils. Geo. Geologic. Eng. 26, 535-542.

Hamm, E., Tapia, F., Melo, F., 2011. Dynamics of shear bands in a dense granular material forced by a slowly moving rigid body. Phys. Rev. E, 84, 041304.

Hanna, A. M., 1981b. Foundations on strong sand overlying weak sand. J. Geot. Geoen. Eng. Div.107, 915-927.

Hanna, A. M., 1982. Bearing capacity of foundations on a weak sand layer overlying a strong deposit. Can. Geo. J. 19, 392-396.

Head, K., 2006. Manual of Soil Laboratory Test. Volume 1: Soil Classification and Compaction Tests, third ed., CRC Press, Boca Raton, FL.

Jahanger, Z. K., Ahmad, A. A., Jahanger, Q. K., 2010. Effect of plate load test curve shape on modulus of subgrade reaction of compacted subbase soil. Pro. Second Ann. Sci. Conf. Coll. Eng., University of Babylon, Iraqi J. Mech. Mat. Eng., E, 1-12.

Jahanger, Z. K., Antony, S. J., Richter, J., 2016. Displacement patterns beneath a rigid beam indenting on layered soil. Pro. Eighth Amer. Reg. Conf. Int. Soc. Terrain-Vehicle Sys. Michigan, USA, Paper No.67.

Jahanger, Z. K., Antony, S. J. 2017. Application of particle image velocimetry in the analysis of scale effects in granular soil. Int. J. Civil Environ. Struct. Constr. Archit. Eng. 11(7), 832-837.

Jahanger, Z. K., Sujatha, J., Antony, S. J., 2018. Local and global granular mechanical characteristics of grain–structure interactions. Indian Geotech J. doi.org/10.1007/s40098-018-0295-5.

Khing, K., Das, B. M., Puri, V. K., Yen, S. C., Cook, E. E., 1994. Foundation on strong sand underlain by weak clay with geogrid at the interface. Geotext. Geomem. 13, 199-206.

Kumar, J., Bhoi, M.K, 2009. Interference of two closely spaced strip footings on sand using model tests. J. Geo. Geoen. Eng. 135, 595-604.

Kumar, J., Kouzer, K., 2007. Effect of footing roughness on bearing capacity factor $N\gamma$. J. Geo. Geoen. Eng. 133, 502-511.

Lau, C. K., 1988. Scale Effects in Tests on Footings, PhD thesis, University of Cambridge, UK.

Lavasan, A. A., Ghazavi, M., 2012. Behavior of closely spaced square and circular footings on reinforced sand. Soi. Found. 52, 160-167.

Lee, H-H., 2015. Finite Element Simulations with ANSYS Workbench 16, SDC publications, USA.

Lee, K. K., Randolph, M. F., Cassidy, M. J., 2013. Bearing capacity on sand overlying clay soils: A simplified conceptual model. Géotechnique 63 (2013) 1285-1297.

Lemmen, H.E., Jacobsz, S.W., Kearsley, E.P., 2017. The influence of foundation stiffness on the behaviour of surface strip foundations on sand. J. South African Instit. Civil Eng., 59(2), 19-27.

Liu, J., Iskander, M., 2004. Adaptive cross correlation for imaging displacements in soils. J. Comput. Civil Eng. 18, 46-57.

Meyerhof G., 1974. Ultimate bearing capacity of footings on sand layer overlying clay. Can. Geo. J. 11, 223-229.

Meyerhof, G., Hanna, A. M., 1978. Ultimate bearing capacity of foundations on layered soils under inclined load. Can. Geo. J. 15, 565-572.

Michalowski, R. L., Shi, L., 1995. Bearing capacity of footings over two-layer foundation soils. J. Geotech. Eng. 121, 421-428.

Mohsenimanesh, A., Ward, S. M., Owende, P. O. M., Javasdi, A., 2009. Modelling of pneumatic tractor tyre interaction with multi-layered soil. Biosys. Eng. 104, 191-198.

Mosadegh, A., Nikraz, H., 2015. Bearing capacity evaluation of footing on a layered-soil using ABAQUS. J. Earth Sci. Clim. Chaange 6:264, 1-8.

Murthy, T. G., Gnanamanickam, E., Chandrasekar, S., 2012. Deformation field in indentation of a granular ensemble. Phys. Rev. E, 85, 061306.

Myslivec, A., Kysela, A. Z., 1978. The Bearing Capacity of Building Foundations, Elsevier, Amsterdam.

Oda, M., Win, S., 1990. Ultimate bearing capacity tests on sand with clay layer. J. Geotech. Eng. 116, 1902-1906.

Okamura, M., Takemura, J., Kimura, T., 1998. Bearing capacity predictions of sand overlying clay based on limit equilibrium methods. Soi. Found. 38.1, 181-194.

O'Loughlin, C., Lehane, B., 2010. Nonlinear cone penetration test-based method for predicting footing settlements on sand. J. Geotech. Geoen. Eng. 136, 409-416.

Prandtl, L., 1920. Über die härte plastischer körper. [On the hardness of plastic bodies] Nachr.kgl. Ges. Wiss. Göttingen, Math.Phys. Kl, 12:74-85 (in German).

Purushothamaraj, P., Ramiah, B. K., Rao, K. V., 1974. Bearing capacity of strip footings in two layered cohesive-friction soils. Can. Geo. J. 11, 32-45.

Ramadan, M. I., Hussein, M. H., 2015. Bearing capacity of sand overlying clay- strip footing. Int. J. Sci. Res. 4, 1852-1859.

Raymond, G.P., Komos, F.E., 1978. Repeated load testing of a model plane strain footing. Can. Geo. J. 15, 190-201.

Shaaban, S., 1983. Evolution of the bearing capacity of dry sand with its density. J. Terramech.20, 129-138.

Shoaei, M. D., Alkarni, A., Noorzaei, J., Jaafar, M. S., Huat, B. B. K., 2012. Review of available approaches for ultimate bearing capacity of two-layered soils. J. Civil Eng. Manage.18, 469-482.

Terzaghi, K., 1943. Theoretical Soil Mechanics, John Wiley and Sons Inc., New York.

Terzaghi, K., Peck, R.B., Mesri, G., 1996. Soil Mechanics in Engineering Practice, third ed. John Wiley and sons, New York.

Vesic, A. S., 1973. Analysis of ultimate loads of shallow foundations. J. Soil Mech. Found. Div. ASCE, 99 (SM1) 45-73.

White, D., Bolton, M., 2004. Displacement and strain paths during plane-strain model pile installation in sand. Géotechnique, 54, 375-397.

White, D., Take, W., Bolton, M., 2003. Soil deformation measurement using particle image velocimetry (PIV), and photogrammetry. Géotechnique, 53, 619-631.

Willert, C. E., Gharib, M., 1991. Digital particle image velocimetry. Exper. Fluids, 10, 181-193.

Yamaguchi, H., 1963. Practical formula of bearing value for two layered ground. Pro. second Asian Reg. Conf. Soil Mech., Japan, 1, 99-105.

CAPTIONS:

Fig. 1. Schematic illustration of the projected area method (Yamaguchi, 1963)

Fig. 2. Failure mode of dense sand overlying loose sand deposit (Hanna, 1981)

Fig. 3. Failure mechanism assumed for sand overlying clay after (Okamura et al. 1998)

Fig. 4. Schematic diagram of failure mechanism underneath the rigid beam on the layered sand using DPIV in the current study

Fig. 5. (a) Experimental setup using DPIV (b) definition of the problem of rigid beam on layered sand, not to scale (c - e) images of the footing in contact with soil for *H/B*=1.0 at q= 0, q= q_{ult} and q> q_{ult} respectively

Fig. 6. Finite element mesh, and an element enlarged for *H/B*=0.5

Fig. 7. Experimental axial load-settlement curves of rigid beam interacting with layered sand. For convenience their corresponding stress and normalised settlement are also presented here

Fig. 8. Effect of depth of dense sand layer overlying loose sand on the evolution of the mean resultant velocity vectors beneath a rigid beam subjected to the ultimate load P_{ult}. Active dead zone (1), radial shear zone (/transition zone) (2) and passive Rankine's zone (3) (Jahanger et al. 2016)

Fig. 9. Comparison of DPIV-based measures with FEM (ANSYS) analysis in layered sand under ultimate load (identical colour codes are used) (left) mean resultant displacement profile (right) vertical displacement component (the field of view is 3*B* (horizontal) × 2.5*B* (vertical))

Fig. 10. Variation of β with *H/B* for strip surface rigid beam on layered sand

Fig. 11. Effect of depth of dense sand layer on (a) ultimate load and (b) UBCR, and their comparison with the theoretical results using modes 1-5

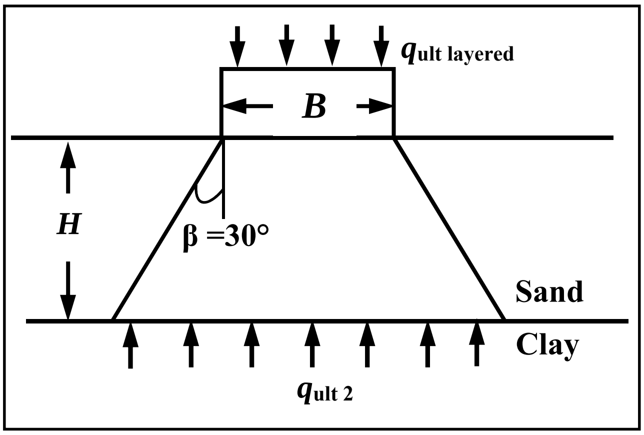

q ult layered
B
H
β =30°
Sand
Clay
q ult 2

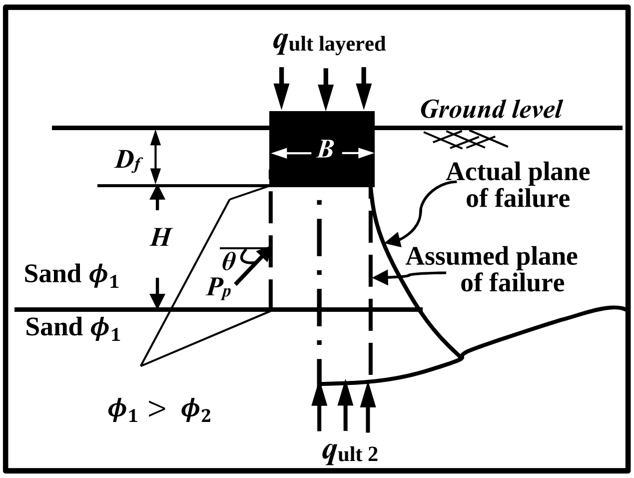

q ult layered
Ground level
B
D_f
Actual plane of failure
H
θ
Assumed plane of failure
Sand ϕ1
P_p
Sand ϕ1
ϕ1 > ϕ2
q ult 2

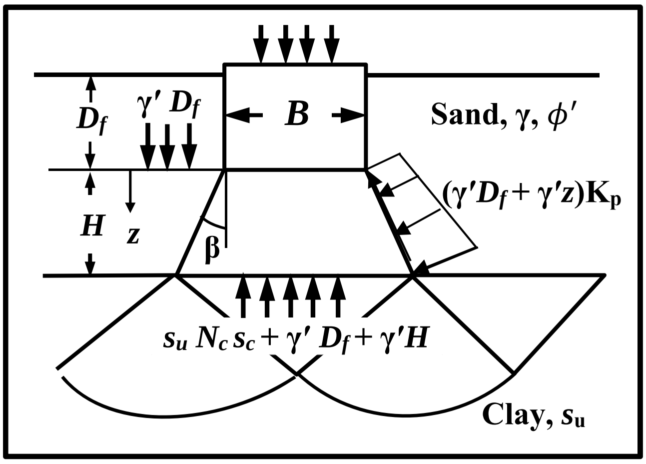

D_f
$\gamma' D_f$
B
Sand, γ, ϕ'
$(\gamma' D_f + \gamma' z)K_p$
H
z
β
$s_u N_c s_c + \gamma' D_f + \gamma' H$
Clay, s_u

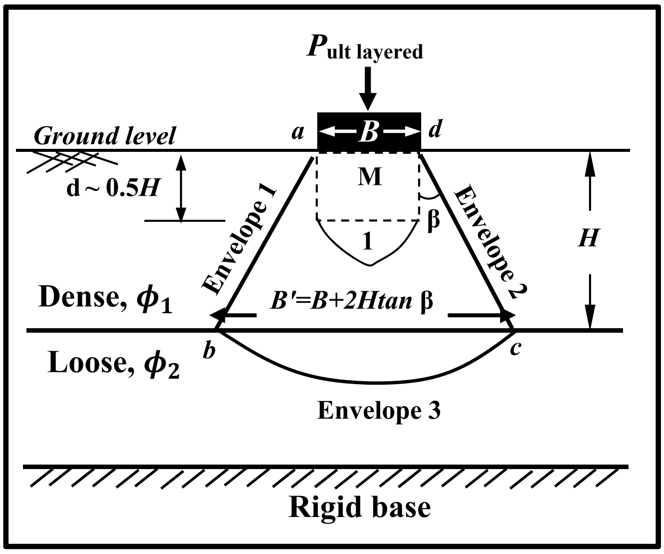

$P_{\text{ult layered}}$
Ground level
a
B
d
d ~ 0.5H
M
1
β
Envelope 1
Envelope 2
H
Dense, ϕ_1
B′=B+2Htan β
b
c
Loose, ϕ_2
Envelope 3
Rigid base

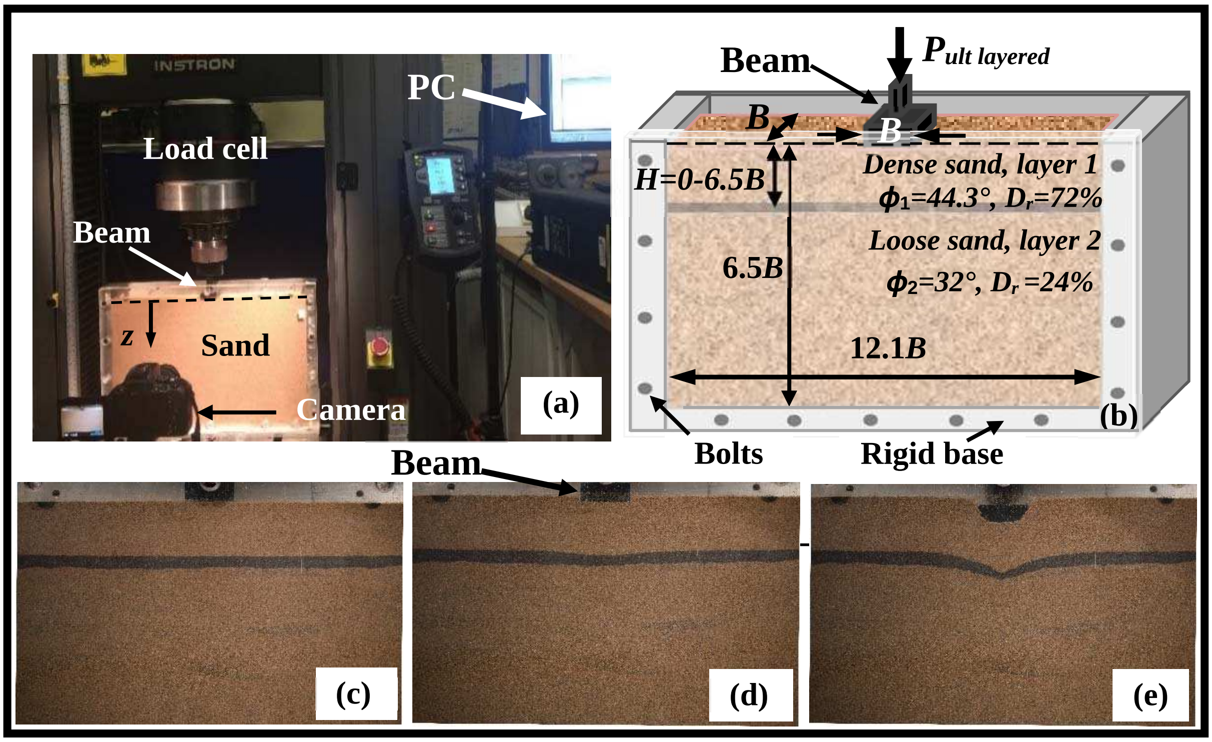
INSTRON
PC
Load cell
Beam
z
Sand
Camera
(a)
Beam
$P_{ult\ layered}$
B
B
H=0-6.5B
Dense sand, layer 1
ϕ_1=44.3°, D_r=72%
Loose sand, layer 2
ϕ_2=32°, D_r=24%
6.5B
12.1B
(b)
Bolts
Rigid base
Beam
(c)
(d)
(e)

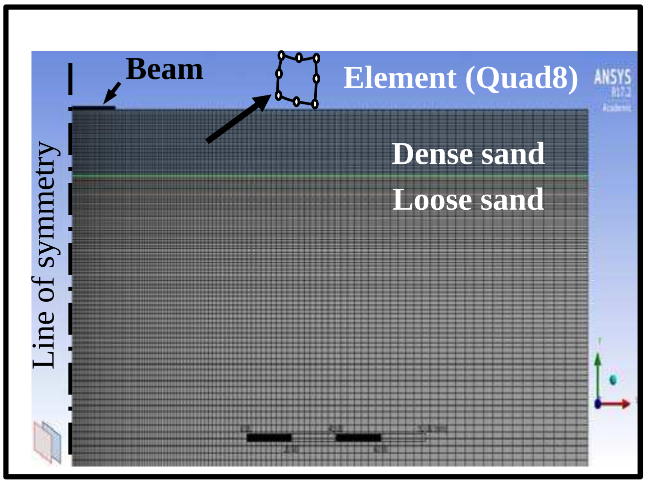

Beam
Element (Quad8)
ANSYS
Dense sand
Loose sand
Line of symmetry

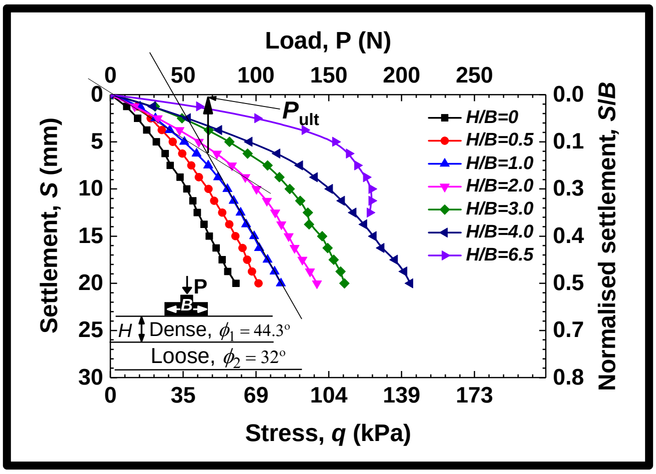

Load, P (N)
0
50
100
150
200
250
P_ult
H/B=0
H/B=0.5
H/B=1.0
H/B=2.0
H/B=3.0
H/B=4.0
H/B=6.5
Settlement, S (mm)
0
5
10
15
20
25
30
Normalised settlement, S/B
0.0
0.1
0.3
0.4
0.5
0.7
0.8
P
B
H
Dense, $\phi_1 = 44.3°$
Loose, $\phi_2 = 32°$
0
35
69
104
139
173
Stress, q (kPa)

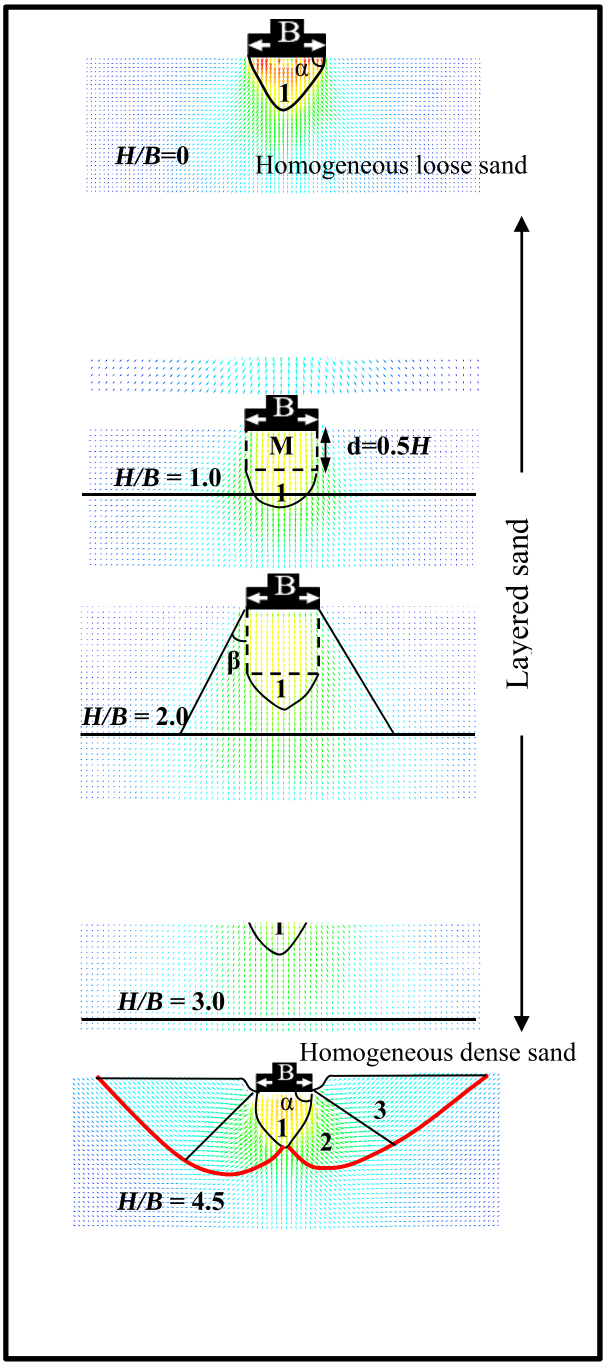
B
α
1
H/B=0
Homogeneous loose sand
B
M
d=0.5H
H/B = 1.0
1
B
β
1
H/B = 2.0
Layered sand
1
H/B = 3.0
Homogeneous dense sand
B
α
1
2
3
H/B = 4.5

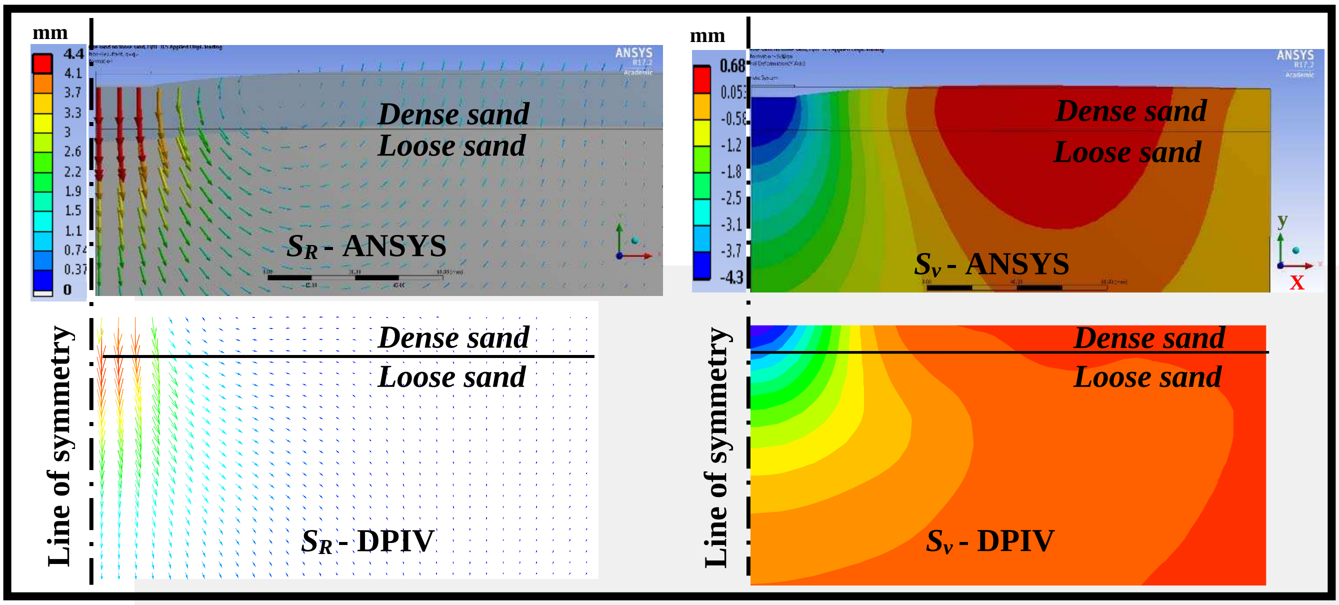
mm
4.4
4.1
3.7
3.3
3
2.6
2.2
1.9
1.5
1.1
0.74
0.37
0
Dense sand
Loose sand
SR - ANSYS
ANSYS
Line of symmetry
Dense sand
Loose sand
SR - DPIV
mm
0.68
0.053
-0.56
-1.2
-1.8
-2.5
-3.1
-3.7
-4.3
Dense sand
Loose sand
Sv - ANSYS
ANSYS
y
x
Line of symmetry
Dense sand
Loose sand
Sv - DPIV

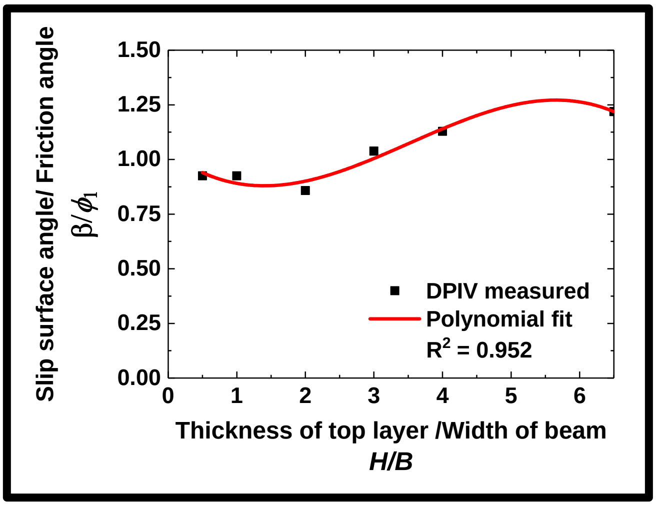
Slip surface angle/ Friction angle
β/ϕ_1
1.50
1.25
1.00
0.75
0.50
0.25
0.00
0
1
2
3
4
5
6
DPIV measured
Polynomial fit
R^2 = 0.952
Thickness of top layer /Width of beam
H/B

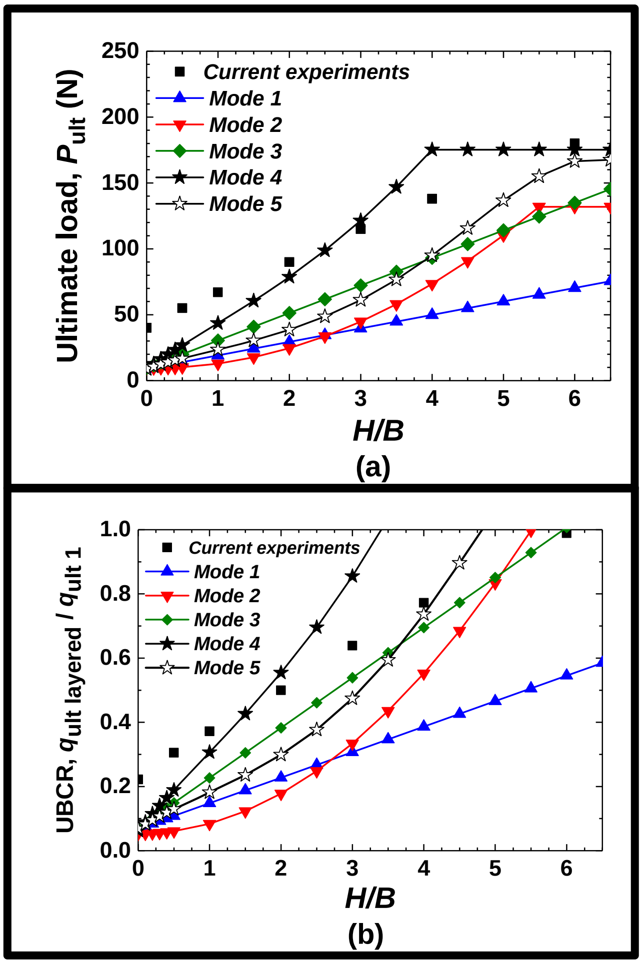

Ultimate load, P_{ult} (N)
Current experiments
Mode 1
Mode 2
Mode 3
Mode 4
Mode 5
H/B
(a)
UBCR, $q_{ult\ layered}$ / $q_{ult\ 1}$
Current experiments
Mode 1
Mode 2
Mode 3
Mode 4
Mode 5
H/B
(b)

Table 1 Experimentally measured physical properties of the sand used.

Type of sand	**Loose**	**Dense**	**Standards**
Dry density (γ_d): (kN/m^3)	14.70	15.80	ASTM C29/C29M
Void ratio (e_o)	0.76	0.64	
Relative density, D_r : % ± 2%	24	72	ASTM C128
Peak angle of internal friction, ϕ_{peak} : °	32	44.3	ASTM D4767
Residual angle of internal friction, ϕ_{cr}: °	30	36.3	Head (2006)
Max. dry density (γ_{dmax}): kN/m^3	16.50		ASTM D698
Min. dry density (γ_{dmin}): kN/m^3	14.23		ASTM D4254 method C
Max. void ratio (e_{max})	0.83		ASTM C29/C29M
Min. void ratio (e_{min})	0.58		ASTM C29/C29M
D_{10} : mm	0.25		
D_{30} : mm	0.31		ASTM D421
D_{50}: mm	0.37		ASTM D422
D_{60} : mm	0.40		
Uniformity coefficient, C_U	1.55		ASTM D2487
Coefficient of curvature, C_C	0.93		
Angle of repose of the sand, °	34		ASTM C1444

Table 2 Comparison of ultimate load results obtained from current DPIV experiments with FEM.

Width of the Footing (mm)	H (mm)	H/B	Ultimate load P_{ult} (N)		
			Current DIPV experiments	FEM	Error %*
38	0	0	40	42	+5
	19	0.5	50	48	-4
	38	1.0	67	71	+5.9
	76	2.0	90	95	+5.5
	114	3.0	115	117	+1.7
	152	4.0	145	148	+2.1
	247	6.5	170	175	+3.0

$* Error\ (\%) = ((FEM - Exp.)/Exp.) \times 100$; (+) overestimated, (-) underestimated